Available online at www.sciencedirect.com
SCIENCE DIRECT®
ELSEVIER
Mechanical Systems and Signal Processing 19 (2005) 447–466
Mechanical Systems and Signal Processing
www.elsevier.com/locate/jnlabr/ymssp

Bicepstrum based blind identification of the acoustic emission (AE) signal in precision turning

Aitzol Iturrospe[a,*], David Dornfeld[b], Vicente Atxa[a], José Manuel Abete[a]

[a] *Mondragon Goi Eskola Politeknikoa, University of Mondragon, Loramendi 4, 20500 Mondragon (Guipúzcoa), Spain*
[b] *Department of Mechanical Engineering, University of California, Berkeley, 5100-A Etcheverry Hall, Berkeley, CA 94720-1740, USA*

Received 5 June 2003; received in revised form 11 December 2003; accepted 22 December 2003

Abstract

It is believed that the acoustic emissions (AE) signal contains potentially valuable information for monitoring precision cutting processes, as well as to be employed as a control feedback signal. However, AE stress waves produced in the cutting zone are distorted by the transmission path and the measurement systems. In this article, a bicepstrum based blind system identification technique is proposed as a valid tool for estimating both, transmission path and sensor impulse response. Assumptions under which application of bicepstrum is valid are discussed and diamond turning experiments are presented, which demonstrate the feasibility of employing bicepstrum for AE blind identification.

Keywords: Acoustic emissions; Higher-order statistics; Blind identification; Precision machining

1. Introduction

During precision machining operations, material is removed from the work-piece at very low depths of cut, being uncut chip thickness usually less than a micrometer. At this scale, high dimensional tolerances are required and nanometer accuracies must be achieved. In order to improve precision, more sophisticated adaptive controls will be needed in the future, as well as new on-line process monitoring sensors and systems, which will feedback the new controls. Nevertheless, monitoring precision cutting processes is difficult by means of some of the sensors that are commonly employed in conventional machining operations. Power consumption,

*Corresponding author. Tel.: +34-943794700; fax: +34-943791536.
E-mail addresses: aiturrospe@eps.monfdragon.edu (A. Iturrospe), dornfeld@me.berkeley.edu (D. Dornfeld), batxa@eps.mondragon.edu (V. Atxa), jmabete@eps.mondragon.edu (J. Manuel Abete).

0888-3270/$ - see front matter
doi:10.1016/j.ymssp.2003.12.006

vibration and force signals show very low sensitivity and signal-to-noise ratio (SNR) for small depths of cut, due to the low-level forces involved in the cutting process. However, the acoustic emissions (AE) signal has proven to be sensitive enough for precision turning monitoring [1].

AE are considered to be transient elastic waves, from 25 kHz to several MHz s, generated by the release of energy from localised sources of materials which are suffering irreversible changes in their structure. During precision metal cutting operations, it is accepted that the main AE sources are plastic deformation, friction and fracture. Thus, AE sources are directly related to the cutting process and the work-piece material properties. Besides, in precision cutting AE signal is less affected by low-frequency mechanical disturbances and the influence of the work-piece material properties is much larger than in conventional machining. In addition, AE signal is detected by simply mounting a piezoelectric transducer on the tool holder, thus, detection of AE signals does not interfere with the cutting process. Therefore, AE technology seems to be promising for precision cutting monitoring.

The AE signal has already been applied to on-line monitoring the process, the tool condition and the surface quality in conventional and precision turning operations. During the late 1970s, different research teams observed that the AE signal was affected by process and tool condition during conventional metal turning operations [2–4]. Since then, a number of, more or less, sophisticated techniques, that make use of the AE signal, have been proposed for monitoring cutting operations. These techniques have been evaluated in several review papers [5–7]. Despite much effort has been directed towards developing on-line condition monitoring systems that make use of features extracted from the AE signal, few of them have shown to be reliable enough as to be implemented in industry. Most of the techniques proposed were based on the root mean square (RMS) value of the AE signal, V_{rms}, as defined by,

$$V_{\mathrm{rms}} = \sqrt{\frac{1}{T}\int_0^T V^2(t)\,\mathrm{d}t},$$

where $V(t)$ is the AE raw signal and T is the integration period. The RMS value carries information of the AE raw signal power during each interval of time, T, reducing the dynamic range and leading to a loss of possibly valuable information. The use of the RMS value can be understood both by the difficulty of working in the high-frequency range of raw AE and by the lack of understanding of AE waves sources and propagation.

Nevertheless, spectral analysis was applied from the very beginning to the AE raw signal, aiming to relate different spectral components or bandwidths mainly to deformation [8] and tool wear [9]. Recently, more sophisticated time–frequency [10] and time-scale [11] techniques have also been proposed for the same purposes. However, AE raw signal spectral analysis has had very limited success, largely due to the following simplifying assumptions.

(a) Most of the times, it has been assumed that the dynamic response of the sensor was flat in its working frequency range.
(b) Most of the times, it has been assumed that spectral components of waves arriving to the AE sensor were directly related to AE sources, such as deformation [12] or friction [13], underestimating the influence of the transmission path filtering.

The objective in this article is to identify variations in the cutting process by monitoring the temporal evolution of the estimated AE transmission path, from the cutting zone to the location where the AE sensor is fixed. In order to estimate transmission path impulse response (IR), bicepstrum based blind identification techniques are presented as a valid tool for this purpose.

This paper is organised as follows. In Section 2, a brief introduction to AE theory and blind identification techniques is presented. First, assumptions taken, related to the AE microscopic source model, the AE transmission path and the measurement system, are discussed. Second, two identification methods are introduced, the complex cepstrum and the bicepstrum. Section 3 describes the experimental procedure used and discusses the results. Finally, conclusions are presented in Section 4.

2. Theoretical considerations

2.1. AE sources in precision turning

During a precision cutting operation, it is accepted that AE are mainly generated by plastic deformation in the primary and secondary zones and by friction related phenomena in the secondary and the tertiary zones [14]. Mechanisms by which AE are produced by dislocations and those which are related to friction are fundamentally different. Nevertheless, stress waves produced by both, a single moving dislocation and those resulting from friction, have been modelled as very short lifetime stress pulses [12,15,16]. These short life pulses are believed to be uncorrelated [17] and their probability density function (PDF) is unknown [18]. Rouby et al. [12] modelled a dislocation AE source as two stress waves with opposite direction, delayed by $\tau = v_0/D$, where v_0 is the speed at which the dislocation is moving between two obstacles on a glide distance, D. Spectral components associated with these very short duration pseudo-oscillatory events would be expected to be in the high MHz or GHz range, as pointed by James and Carpenter [16], far beyond commercially available piezoelectric AE sensor frequency range. Stephens and Pollock [15] argued that an oscillatory or double pulse model has a mean value of zero and leads to no change in the static stress level. However, AE are produced during irreversible changes in the material. Therefore, they proposed a single stress pulse AE source model. The frequency spectrum of such a source will have a maximum value at zero frequency and a nearly flat power spectral density along the piezoelectric sensor bandwidth.

2.2. Transmission path and measurement system

Stress waves generated by the AE source pulses propagate from the cutting point to the sensor location, being distorted by the transmission path. During propagation, these waves suffer multiple reflections, mode conversions and attenuation. AE waves will also excite the resonances in small specimens [15], due to the broadband nature of the single pulse stress source.

Therefore, a model for the transmission path seems to be necessary in order to equalise the distorted stress waves arriving to the sensor location. Nevertheless, a priori knowledge of the transmission path characteristics is impracticable for most of the applications. Indeed, modelling the propagation of elastic waves through structures and specimens has been accomplished both

analytically [19] and numerically by means of finite element analysis (FEA) [20]. However, analytical approaches are restricted to simple geometries and, the computational cost and the difficulty for defining material properties and boundary conditions, have limited results obtained by FEA.

Besides, it seems reasonable to think that changes in cutting conditions, such as tool wear, chip length contact or material properties of the work-piece, would lead to a change in the direction of produced stress waves. Changes in the direction of the sources will lead to different propagation paths for the AE waves. Therefore, an on-line estimation for the transmission system seems to be more appropriate because it has potentially useful information about the source events.

In addition to the transmission path filtering, distortion caused by the measurement system response is also of consideration, especially when piezoelectric sensors are employed. The reason is that piezoelectric sensors high sensitivity is achieved by one single or multiple resonances spread along their working bandwidth.

2.3. A linear time invariant (LTI) model for blind system identification

Transmission path and piezoelectric sensor response have traditionally been modelled as LTI systems in ultrasonic non-destructive testing (NDT) applications [21]. The same kind of model is taken in this article for an AE monitoring application. It is assumed that both path transmission and sensor response are time invariant over a suitable observation period or only change slightly. In this model, the measured AE signal, $y(t)$, results from the convolution of the excitation due to cutting process, $p(t)$, with the path IR, $h_m(t)$, and the a AE sensor and measurement system IR, $h_S(t)$, as shown

$$y(t) = h_S(t) * h_m(t) * p(t) + n(t), \tag{1}$$

where $*$ denotes convolution and $n(t)$ is added to the system output and it is assumed to be zero mean white Gaussian noise due to the measurement system. A block diagram of the model is given in Fig. 1.

Conventional deconvolution methods applied in ultrasonic NDT, such Wiener filter and minimum variance deconvolution [22], require a priori knowledge of both input, $p(t)$, and output, $y(t)$, in order to estimate the transfer function. Since only the output data is available in the case of AE, system model must be estimated from the output, $y(t)$, by taking some statistical assumptions for the excitation process. This kind of procedure is referred as blind identification.

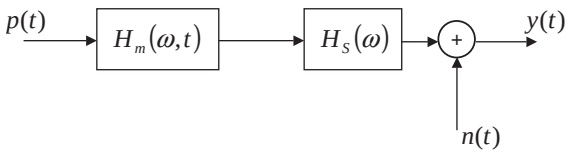

Fig. 1. LTI model for an AE monitoring application.

2.4. Complex cepstrum based blind identification

Let consider an autoregressive moving average (ARMA) energy sequence, $h(k)$, which Z transform is,

$$H(z) = Kz^{-r} I(z^{-1}) O(z) \tag{2}$$

with

$$I(z^{-1}) = \frac{\prod_{i=1}^{L_1}(1 - a_i z^{-1})}{\prod_{i=1}^{L_3}(1 - d_i z^{-1})}, \tag{3}$$

$$O(z^{-1}) = \prod_{i=1}^{L_2}(1 - b_i z^{-1}), \tag{4}$$

where K is a constant, r is a integer, $I(z)$ is the minimum phase component and $O(z)$ is the maximum phase component. The cepstral parameters, $A^{(m)}$ and $B^{(m)}$, are given by

$$\begin{aligned} A^{(m)} &= \sum_{i=1}^{L_1} a_i^m - \sum_{i=1}^{L_3} d_i^m, \\ B^{(m)} &= \sum_{i=1}^{L_2} b_i^m. \end{aligned} \tag{5}$$

The complex cepstrum was defined by Oppenheim and Shaffer [23] as

$$c_h(m) = Z^{-1}[\log[H(z)]] \tag{6}$$

and it has been demonstrated elsewhere [24] that it is related to the cepstral parameters, $A^{(m)}$ and $B^{(m)}$ as,

$$c_h(m) = \begin{cases} \log|A|, & m = 0, \\ -\dfrac{A^{(m)}}{m}, & m > 0, \\ \dfrac{B^{(-m)}}{m}, & m < 0. \end{cases} \tag{7}$$

It can also be demonstrated [24] that the IR for the minimum phase component, $i(k)$ and the maximum phase component, $o(k)$, of $H(z)$ can be obtained from the cepstral parameters by means of

$$i(k) = -\frac{1}{k}\sum_{m=2}^{k+1} A^{(m-1)} i(k - m + 1), \quad k \geqslant 1, \tag{8a}$$

$$o(k) = \frac{1}{k} \sum_{m=k+1}^{0} B^{(1-m)} o(k-m+1), \quad k \leqslant -1 \tag{8b}$$

taking $i(0) = o(0) = 1$. Finally, the system IR is obtained convolving both minimum phase and maximum phase IRs, $h(k) = i(k) * o(k)$.

The complex cepstrum is a homomorphic transformation that satisfies the generalised principle of superposition [25]. It has been applied to separate signals that have been combined by convolution, first by transforming convolution into product by the Z transform, then by transforming product into sum by taking the logarithm and finally returning to the time domain by the inverse Z transform. If the convolved signals have frequency components concentrated in different ranges, signal separation is achieved taking a cut-off time and zeroing, or *liftering,* the high time complex cepstrum (filtering the low-frequency components) or the low time components (filtering the high time frequencies).

Rice and Wu [26] proposed the complex cepstrum as a technique to accomplish the deconvolution of AE signal during interrupted milling operations. They assumed that AE bursts during this process were associated with the fracture phenomena. Each of these bursts was modelled at the source as a deterministic wavelet, with frequency components in the range of the AE sensor. These wavelets were then convolved with the transmission path IR, consisting of multiple echoes. Rice and Wu assumed that low time components in the complex cepstrum domain were related to the source wavelet. They took a cepstral cut-off and high time *liftered* the complex cepstrum, so that the components related to the transmission path were removed. Then, the source wavelet was reconstructed by computing the inverse complex cepstrum after high liftering the complex cepstrum.

However, for the complex cepstrum to be valid as a deconvolution technique, the combined signals need to have their spectral energy concentrated at different frequency ranges. Moreover, the complex cepstrum can only be applied when excitation signals are deterministic. Certainly, this seems not to be the case for diamond precision turning. Indeed, the process excitation signal is more likely to be a random flat spectrum white noise in the sensor frequency range as stated in Section 2.1.

2.5. Bicepstrum based blind identification

Bicepstrum has already been successfully utilised as a technique for blind deconvolution in many seismic and ultrasonic applications [27]. The bicepstrum is defined in Eq. (9), as the inverse 2D Z transform of the log bispectrum, $C_3^H(z_1, z_2)$, and it is related to the cepstral parameters by Eq. (10). See Appendix A for a brief introduction of the bispectrum properties

$$b_H(m,n) = Z_2^{-1}[\log[C_3^H(z_1, z_2)]], \tag{9}$$

$$b_h(m,n)=\begin{cases}\log|A^3|, & m=0,\ n=0,\\ -\dfrac{1}{n}A^{(n)}, & m=0,\ n>0,\\ -\dfrac{1}{m}A^{(m)}, & n=0,\ m>0,\\ \dfrac{1}{m}B^{(-m)}, & n=0,\ m<0,\\ -\dfrac{1}{n}B^{(-n)}, & m=0,\ n<0,\\ -\dfrac{1}{n}B^{(n)}, & m=n>0,\\ \dfrac{1}{n}A^{(-n)}, & m=n<0,\\ 0, & \text{otherwise.}\end{cases} \tag{10}$$

Let $H(z)$ be a LTI system driven by a zero-mean, independent identically distributed (i.i.d.) signal with skewness, γ_3^p (see Appendix A). Then, its bispectrum, $C_3^H(z_1,z_2)$, exists and is given by

$$C_3^H(z_1,z_2)=\gamma_3^p H(z_1)H(z_2)H(z_1^{-1}\cdot z_2^{-1}). \tag{11}$$

Without loss of generality, it can be assumed that $\gamma_3^p=1$ in order to identify $H(z)$ phase and magnitude relation among the different spectral components, because it will be embedded as a constant in the bispectrum.

The bicepstrum can be applied to deconvolve both deterministic and stochastic signals [27]. Bicepstrum contains phase information and it can be applied to obtain the system IR and the inverse filter. Another advantage of bicepstrum based blind identification is that the bispectrum of a zero skewness signal is zero, thus, bispectrum filters any additive Gaussian noise term (see Ref. [27] and Appendix A). The bicepstrum can be used for minimum and non-minimum white-noise non-zero skewness driven LTI system blind identification and it does not require a priori knowledge of the order of the system to be identified. Moreover, the inverse IR, $f(k)$, could be easily computed from the cepstral parameters obtained from the bicepstrum by means of

$$f_i(k)=-\frac{1}{k}\sum_{m=2}^{k+1}[-A^{(m-1)}]f_i(k-m+1),\quad k\geqslant 1, \tag{12a}$$

$$f_0(k)=\frac{1}{k}\sum_{m=k+1}^{0}[-B^{(1-m)}]f_0(k-m+1),\quad k\leqslant -1 \tag{12b}$$

taking $f_i(0)=f_0(0)=1$ and then convolving, $f(k)=f_i(k)*f_0(k)$.

3. Experiments

3.1. AE sensor calibration

In order to evaluate the relative influence of propagation path and sensor response in the AE signal spectrum, two different tests were carried out. For the first test, two SE-900-MWB Deci, Inc. AE sensors were positioned face-to-face and coupled with petroleum jelly, one of them acting as a transmitter and the other one as a receiver (Fig. 2a). The driving transducer was excited by constant amplitude sinusoidals. Frequencies from 1 up to 500 kHz were swept with steps of 100 Hz. The excitation signal was generated with a HP33120A function generator. The output signal from the receiver sensor was first amplified (40 dB) and filtered from 20 kHz to 1 MHz with the AESMART302A signal conditioner, and then digitalised at a 2 MHz sampling frequency with a 12 bits Adlink PCI9812 acquisition card. For the second test, both sensors were separated by a $1 \times 1 \times 5$ in size beam and coupled with petroleum jelly to the same face of the beam, as shown in Fig. 2b. Both tests were repeated 10 times and the average frequency magnitude response for both tests is shown in Fig. 3, where an averaged version curve of the response obtained in the second test is included.

Fig. 3 shows that the frequency response of the SE-900-MWB AE sensor has three mean lobes in the range from 25 up to 500 kHz centred at 133, 295 and 430 kHz. One large resonance at 295 kHz, and several peaks located at 34, 120, 175, 290 and 430 kHz.

As it can be observed in Fig. 3, for the second test, the obtained power spectrum is largely influenced by the sensor frequency response. Nevertheless, superposed to it there are multiple

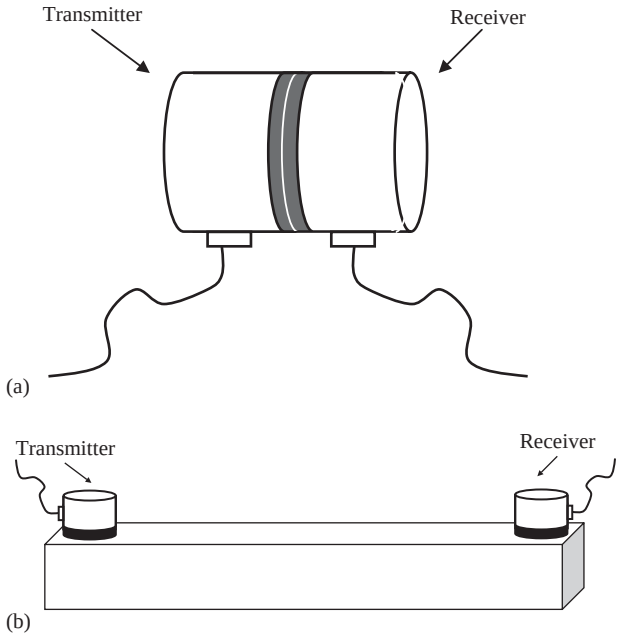

Fig. 2. (a) Sensors positioned face-to-face, (b) sensors separated by a beam.

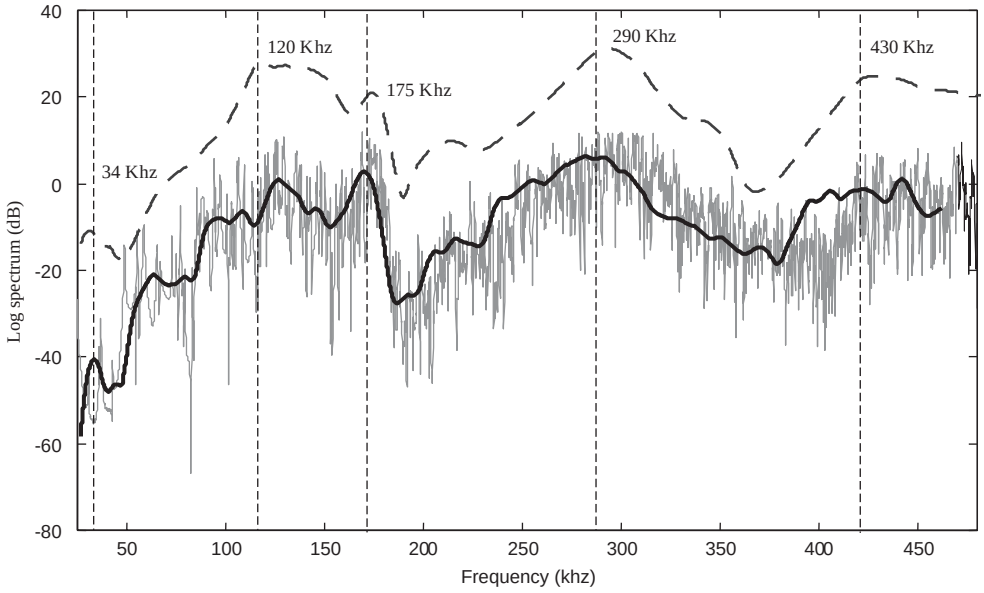

Fig. 3. Magnitude frequency response for sensors separated by a beam (thin solid line). Averaged version of the magnitude frequency response for sensors separated by a beam (thick solid line). Magnitude frequency response for sensors positioned face-to-face (dashed line).

peaks that can be attributed to the transmission path transfer function. Attenuation in the second test is also attributed to AE transmission through the interposed beam. Therefore, AE spectra seems to be primarily determined by sensor response and transmission path.

3.2. Precision turning experiments

3.2.1. Experimental set-up

A series of experiments were conducted in order to verify the validity of bicepstrum for AE signal blind deconvolution during precision diamond turning. Experiments were conducted on a Rank Pneumo MSG-326 precision lathe, equipped with an air-bearing spindle and precision air-bearing lays. An HP laser interferometer was used to measure tool position in the feed direction, and a Heidenhain linear encoder for measuring spindle rotation angle. Material was single crystal (1 1 1) orientation Cu, grown via the Bridgman technique, rated at 5 N (99.999% pure). The work-piece was clamped onto the spindle of the lathe by means of vacuum and machined by a single crystal diamond tool with 0° rake angle, 10° clearance angle, 0.274 μm nose radius. Cutting parameters were maintained constant in all tests to 1000 rpm, 21.6 μm/rev feed and a nominal depth of cut of 2 μm. Cutting zone was continuously lubricated with alcohol during cutting operation. The measurement system was the same as that described for the calibration preliminary tests and both, encoder pulses and AE raw signal, were low pass filtered to prevent aliasing and continuously digitalised at a 1.2 MHz sampling frequency during three cycles of the spindle in each test. Signals were acquired from three different sensor locations, A, B and C, one on the tool-holder and two on the tool-post, as it can be seen in Fig. 4. The AE signals were measured by one

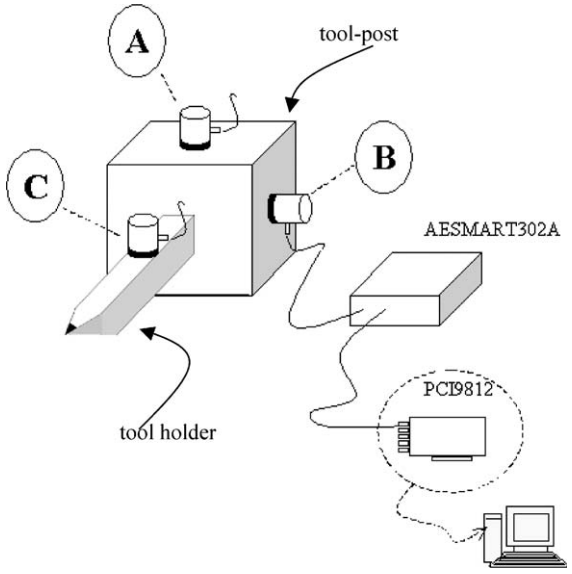

Fig. 4. Sensor locations and measurement system.

SE-900-MWB Deci Inc. sensor which was fixed onto the different positions by means of a mixture of petroleum jelly and glue.

3.2.2. Results and discussion

The strategy followed was first to estimate the whole IR from the cutting point, including transmission path and sensor transfer functions. Then, the Fourier transform of the estimated IR was compared with the sensor response, which it was known because it was previously obtained by calibration in Section 3.1.

It was assumed that measured data, $y(t)$, was a convolution of the excitation process, $p(t)$, with the combined transmission path and the sensor IR, $h_{ms}(t)$,

$$y(t) = h_{ms}(t) * p(t) + n(t), \tag{13}$$

where $n(t)$ is a zero skewness white noise and $p(t)$ is a i.i.d. non-zero skewness white noise due to the measurement system. This assumption of zero skewness for the added noise was experimentally demonstrated. AE signal was recorded when the lathe was completely turned on but no cutting operation was taking place. The AE signal power spectral density was observed to be flat for the acquired noise signal and the Hinich's test was performed [28] in order to find out whether if the noise PDF had zero skewness. According to the Hinich's test the noise signal had zero skewness with 1% error probability.

Data collected during each test was divided in successive 10 segments of 1024 samples and cepstral parameters were calculated for each set. The 2D fast Fourier transform (FFT2) method (see Ref. [24] and Appendix B) described by Eq. (14) was utilised for computational efficiency to compute the bicepstrum,

$$n \cdot b_H(n,m) = F_2^{-1}\left\{\frac{F_2[n \cdot m_3^H(n,m)]}{F_2[m_3^H(n,m)]}\right\}, \tag{14}$$

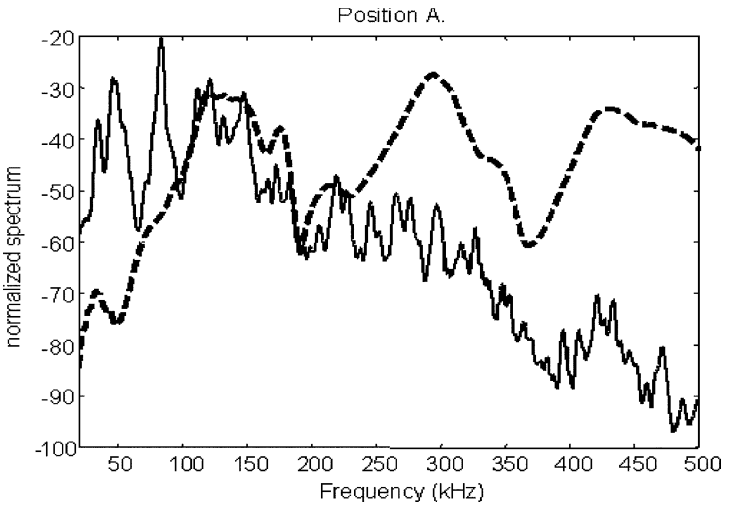

Fig. 5. Log magnitude spectrum for location A (solid line) compared to the log magnitude response for the SE-900-MWB sensor attenuated 70 dB (dashed line).

where $m_3^H(n,\ell)$ is the third-order moment function, $F_2[\cdot]$ is the FFT2 and $F_2^{-1}[\cdot]$ is the inverse FFT2. The FFT2 estimation method is recommended for systems with pronounced resonances [24]. Then, cepstral parameters were calculated by means of Eq. (10), which were employed to compute the estimated system IR, $h_{ms}(t)$ by means of Eq. (8).

Some results are shown in Figs. 5–7, where the magnitude frequency responses obtained by the Fourier transform of the estimated IRs are illustrated, for the three different sensor locations. It can be observed that the sensor response still influences the estimated log spectrum, especially when the sensor is positioned directly on the tool holder (Fig. 7). In the same figure, it can also be observed that high-frequency AE waves are much less attenuated than when the sensor is fixed far from the cutting point (positions A and B). For the three different sensor locations, apart from the influence of the sensor response, there are several peaks along the whole analysed frequency range. It is to be mentioned the energy of those peaks located in the low-frequency range, up to 100 kHz, where sensor response is expected to be poor.

It is clear that the estimated frequency responses differ not only from the sensor frequency response function but also from one sensor location to another. It can be argued that these differences could be related to the mechanical system vibration modes excited by the cutting process. The excited mechanical system modes influence changes from one sensor location to another, which is the same as saying that the transmission path differs from one location to another. Especially, it must be emphasised the low-frequency range peaks which could be attributed to a larger influence of the lower frequency mechanical modes. On the other hand, the magnitude of some of the peaks change depending on where the sensor was fixed on, due to variations in the transmission path. Respecting attenuation, it must be mentioned that the mechanical system generally acts as a low-pass filter for the AE waves. When the sensor is fixed on the tool post, the distance between the cutting point and the sensor location is larger and AE waves go through an interface in their way to the sensor. Therefore, attenuation for high

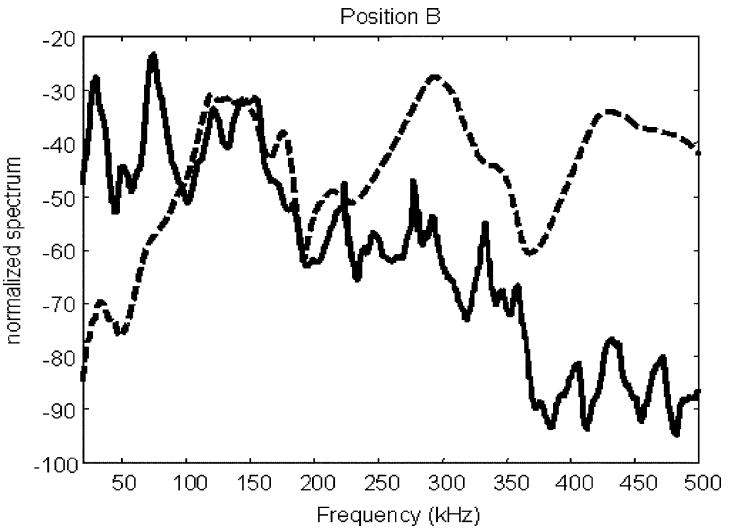

Fig. 6. Log magnitude spectrum for location B (solid line) compared to the log magnitude response for the SE-900-MWB sensor attenuated 70 dB (dashed line).

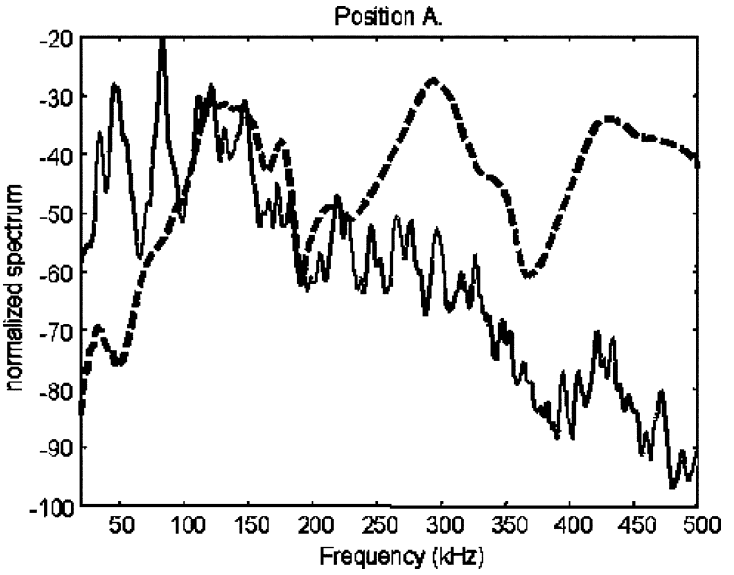

Fig. 7. Log magnitude spectrum for location C (solid line) compared to the log magnitude response for the SE-900-MWB sensor attenuated 70 dB (dashed line).

frequencies is larger as it can be observed in Figs. 5 and 6 (positions A and B, respectively). On the contrary, for Fig. 7, where the sensor is positioned directly on the tool holder, high-frequency AE waves are much less attenuated and the influence of the sensor response can be better appreciated in the high-frequency range.

Table 1
Natural frequencies for the tool-holder

Mode	Frequency (Hz)
1	8066
2	8326
3	30,857
4	39,059
5	39,571
6	48,994
7	79,234
8	88,709
9	91,908
10	92,131

3.2.2.1. Comparison with tool-holder natural frequencies. In order to find out whether if any of these peaks are really related to tool-holder modes. A finite element model for a fixed tool-holder was developed and a numerical modal analysis was performed by FEA, using IDEAS as FEA software. Boundary conditions were taken so that tool-holder nodes in contact with the support had restrained all the translations while the rotations were free. The type of elements utilised were solid elements of parabolic order. Most of the elements were 1 mm side bricks. Natural frequencies were obtained up to 100 kHz, which are listed in the table bellow.

Despite results of the numerical modal analysis can only be interpreted in a qualitative manner, due to the simplifications taken, it is at least shown in Table 1 that tool-holder modes higher than the second one are in the frequency range associated with AE.

Fig. 8 compares the magnitude of the Fourier transform of the estimated IR, for the test when the sensor was fixed directly on the tool-holder, with the natural frequencies associated with the tool-holder modes up to 100 kHz. In this figure there can be observed three main peaks at 34, 49 and 75 kHz.

While the spectral peak centred on 34 kHz could be associated with a sensor resonance (see Fig. 3), both the peak at 49 kHz and that located at 75 kHz are associated to the mechanical system mode 3 and mode 6, respectively. These peaks correspond to those modes that contribute significantly to surface displacements at the sensor location. The rest of the modes have no relative influence at the sensor location.

3.2.2.2. Influence of process variations in the transmission path. Positioning the AE sensor on different location will certainly change the transmission path for the AE produced in the cutting zone. The question that arises is whether if the estimation of the IR is sensible enough for monitoring variations in the process. These variations would modify the distribution of the AE sources directions, so that the propagation paths would be affected.

Although exhaustive tests were not conducted to demonstrate this relation between process condition and the transmission path IR, time evolution for the ratio between spectral energy concentrated around two distinctive peaks was analysed. These two peaks, at 49 kHz and at 75 kHz, were observed when positioning the sensor on the tool-holder and they can not be

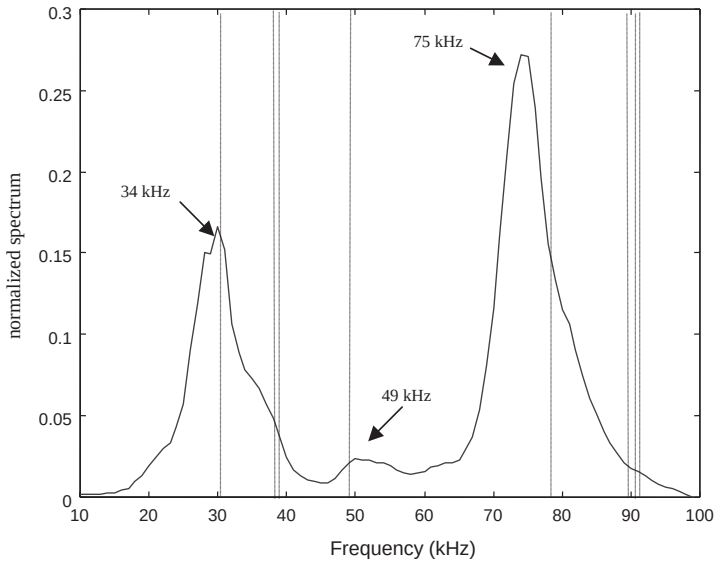

Fig. 8. Estimated frequency response (solid curve) and location for the tool-holder natural frequencies calculated by FEA (vertical lines).

attributed to sensor resonances as it can be observed in Fig. 3. The AE energy changed cyclically with a period equal to 120° of the spindle rotation angle during the all tests. This cyclic change could be attributed to a change in the cutting forces due to different crystal orientation during one rotation [29]. Fig. 9 shows how variations in the ratio seem to be correlated the variations in the AE raw signal and the AE RMS value. The ratio in Fig. 9 is scaled so that it can be compared to the variations in the AE energy.

Taking the following assumptions: that spectral and statistical properties of excitation, sensor response is time invariant and linear and that mechanical system properties do not vary significantly with time. Then, estimated IR spectral variations should only be attributed to variations in the direction of excitation, and therefore to changes in the propagation path. In the present experimental study, excitation direction has changed due to variation of the work-piece crystal orientation. Nevertheless, the same blind identification technique could be used in the future for detecting and monitoring variations in the cutting process which are supposed to change the direction of the excitation, such as increase in the tool wear.

4. Conclusions

Precision diamond turning condition monitoring by means of AE has been presented as a blind identification problem. A bicepstrum based technique has been proposed for obtaining the transmission path IR.

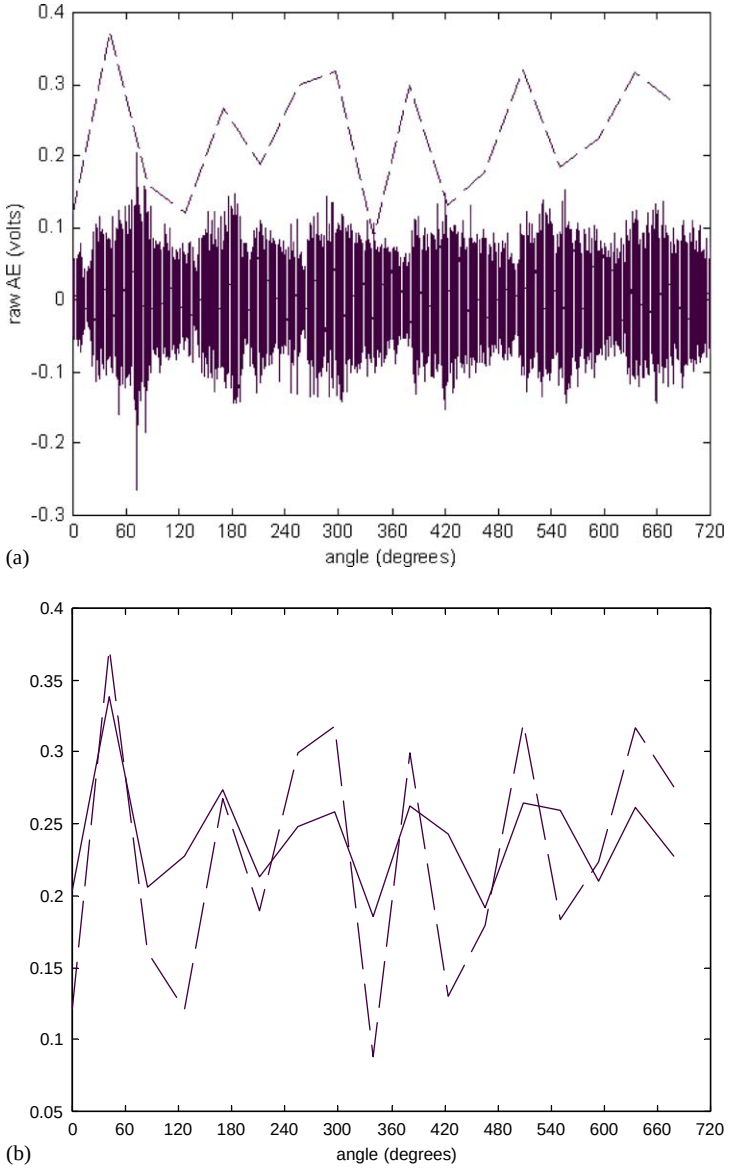

Fig. 9. (a) AE raw signal (solid line) and ratio between two spectral peaks located at 49 and 75 kHz (dashed line). (b) Normalised AE RMS signal (solid line) and normalised ratio between two spectral peaks located at 49 and 75 kHz (dashed line).

Experimental tests and FEA simulations have been conducted which demonstrate that AE raw signal spectral characteristics are, to a great extent, influenced by the transmission path and the sensor response.

The bicepstrum is a valid tool for obtaining the transmission path transfer function under the assumption taken in this article.

Finally, it has been experimentally observed that AE transmission path IR change with variations in the cutting conditions.

Acknowledgements

This work has been partially supported by the University and Research Department of Basque Country Government (PI 2001-15) and by the Spanish Ministry of Science and Technology (project DPI 2002-04386-C02-02).

The authors would also like to acknowledge the detailed and constructive comments of the reviewers, as well as appreciate their helpful suggestions and criticisms.

Appendix A

A.1. Moments and cumulants for random variables

Given a set of n real random variables $\{x_1, x_2, \ldots, x_n\}$ their joint moments of order $r = k_1 + k_2 + \cdots + k_n$ are defined as

$$Mom[x_1^{k_1}, x_2^{k_2}, \ldots, x_n^{k_n}] = E\{x_1^{k_1} x_2^{k_2} \ldots x_n^{k_n}\}(-j)^r \left.\frac{\partial^r \Phi(\omega_1, \omega_2 \ldots \omega_n)}{\partial\omega^{k_1}\partial\omega^{k_2}\ldots\partial\omega^{k_n}}\right|_{\omega_1=\omega_2=\cdots\omega_n=0}, \tag{A.1}$$

where $\Phi(\omega_1, \omega_2 \ldots \omega_n) = E\{e^{j(\omega_1 x_1 + \omega_2 x_2 + \cdots + \omega_n x_n)}\}$ is their joint characteristic function.

The joint cumulants of order r of the same set of random variables are defined as follows:

$$Cum[x_1^{k_1}, x_2^{k_2}, \ldots, x_n^{k_n}] = (-j)^r \left.\frac{\partial^r \ln \Phi(\omega_1, \omega_2 \ldots \omega_n)}{\partial\omega^{k_1}\,\partial\omega^{k_2}\ldots\partial\omega^{k_n}}\right|_{\omega_1=\omega_2=\cdots\omega_n=0}. \tag{A.2}$$

An important property of cumulants is that if a set of random variables $\{x_1, x_2, \ldots, x_n\}$ is jointly Gaussian, all joint cumulants of order $n > 2$ are identical to zero.

A.2. Moments and cumulants of stationary processes

Let $\{X(k)\}$, with $k = 0, \pm 1, \pm 2, \ldots$, be a real stationary random process and its moments up to order n, m_n^X, exist and be defined, depending on time differences, by,

$$\begin{aligned} m_n^X(\tau_1, \tau_2, \ldots, \tau_{n-1}) &= Mom[X(k), X(k+\tau_1), \ldots, X(k+\tau_{n-1})] \\ &= E\{X(k)X(k+\tau_1)\ldots X(k+\tau_{n-1})\} \end{aligned} \tag{A.3}$$

and its cumulants up to order n by,

$$c_n^X(\tau_1, \tau_2, \ldots, \tau_{n-1}) = Cum[X(k), X(k+\tau_1), \ldots, X(k+\tau_{n-1})]. \tag{A.4}$$

Combining Eqs. (A.2)–(A.4) the following relationship between first-, second- and third-order cumulants and moments can be obtained,

$$c_1^X = m_1^X = E\{X(k)\} \quad \text{(mean value)}, \tag{A.5}$$

$$c_2^X = m_2^X(\tau_1) - (m_1^X)^2 \quad \text{(covariance sequence)}, \tag{A.6}$$

$$\begin{aligned} c_3^X(\tau_1,\tau_2) = {} & m_3^X(\tau_1,\tau_2) - m_1^X[m_2^X(\tau_1) \\ & + m_2^X(\tau_2) + m_2^X(\tau_2-\tau_1)] + 2(m_1^X)^3 \\ & \text{(third-order cumulant sequence)}. \end{aligned} \tag{A.7}$$

According to Eqs. (A.6) and (A.7), for a zero-mean stationary random process, second- and third-order cumulants are equal to second- and third-order moments, respectively.

Zeroing $\tau_1 = \tau_2 = \tau_3 = 0$ in Eqs. (A.6) and (A.7) and by putting $m_1^X = 0$ we obtain the variance and the skewness for process $\{X(k)\}$, which are defined as follows:

$$\gamma_2^X = E\{X^2(k)\} = c_2^X(0) \quad \text{(variance)},$$

$$\gamma_3^X = E\{X^3(k)\} = c_3^X(0,0) \quad \text{(skewness)}.$$

A.3. Cumulant spectra: bispectrum

The nth order cumulant spectrum for a real strictly stationary process, $\{X(k)\}$, is defined as,

$$\begin{aligned} & C_n^X(\omega_1,\omega_2,\ldots,\omega_{n-1}) \\ & \quad = \sum_{\tau_1=-\infty}^{+\infty} \cdots \sum_{\tau_{n-1}=-\infty}^{+\infty} c_n^X(\tau_1,\tau_2,\ldots,\tau_{n-1}) \mathrm{e}^{-j(\omega_1\tau_1+\omega_2\tau_2+\cdots+\omega_{n-1}\tau_{n-1})}, \end{aligned}$$

$|\omega_i| \leqslant \pi$, for $i = 1,2,\ldots,n-1$ and $|\omega_1+\omega_2+\cdots+\omega_{n-1}| \leqslant \pi$.

Particular cases of cumulant spectra are power spectrum ($n = 2$) and bispectrum ($n = 3$). In the same way that power spectrum is defined as the second-order cumulant spectrum by,

$$C_2^X(\omega) = \sum_{\tau=-\infty}^{\infty} c_2^X(\tau)\mathrm{e}^{-j\omega\tau} \quad \text{with } |\omega| \leqslant \pi$$

bispectrum is defined as the third-order cumulant spectrum as follows:

$$C_3^X(\omega_1,\omega_2) = \sum_{\tau_1=-\infty}^{\infty} \sum_{\tau_2=-\infty}^{\infty} c_3^X(\tau_1,\tau_2)\mathrm{e}^{-j(\omega_1\tau_1+\omega_2\tau_2)}$$

$$|\omega_1| \leqslant \pi, \quad |\omega_2| \leqslant \pi \quad \text{and} \quad |\omega_1+\omega_2| \leqslant \pi, \tag{A.8}$$

where $c_3^X(\tau_1,\tau_2)$ is the third-order cumulant sequence described by Eq. (A.7). From moment properties [27] and Eq. (A.7) it can be demonstrated the following symmetries for $c_3^X(\tau_1,\tau_2)$:

$$\begin{aligned} c_3^X(\tau_1,\tau_2) & = c_3^X(\tau_2,\tau_1) = c_3^X(-\tau_2,\tau_1-\tau_2) \\ & = c_3^X(\tau_2-\tau_1,-\tau_1) = c_3^X(\tau_1-\tau_2,-\tau_2) \\ & = c_3^X(-\tau_1,\tau_2-\tau_1). \end{aligned}$$

By these symmetry properties and the definition of bispectrum, we can also obtain a series of symmetries for the bispectrum, as follows:

$$\begin{aligned} C_3^X(\omega_1,\omega_2) &= C_3^X(\omega_2,\omega_1) = C_3^X(-\omega_2,-\omega_1) \\ &= C_3^X(-\omega_1-\omega_2,\omega_2) = C_3^X(\omega_1,-\omega_1-\omega_2) \\ &= C_3^X(-\omega_1-\omega_2,\omega_1) = C_3^X(\omega_2,-\omega_1-\omega_2). \end{aligned}$$

Therefore knowledge of the bispectrum in the region $\omega_2 \geqslant 0$, $\omega_1 \geqslant \omega_2$ and $\omega_1+\omega_2 \leqslant \pi$, is enough to define the entire bispectrum.

A.4. Bispectrum of non-Gaussian linear processes with additive Gaussian noise

Let $H(\omega)$ be the frequency response of a finite dimensional exponentially stable LTI system function, as defined by Eqs. (2)–(4), and the system input, $X(\omega)$, be a stationary non-Gaussian process, white, i.i.d., with skewness γ_3^X. Let also consider its output is corrupted by an additive Gaussian noise, $N(\omega)$, as follows:

$$Y(\omega) = H(\omega)X(\omega) + N(\omega).$$

Then the bispectrum of its output with an additive Gaussian noise, $Y(\omega)$, is given in the frequency domain [27] by,

$$C_3^Y(\omega_1,\omega_2) = \gamma_3^X H(\omega_1)H(\omega_2)H^*(\omega_1+\omega_2) + C_3^W(\omega_1,\omega_2). \tag{A.9}$$

As we have assumed that $N(\omega)$ is Gaussian, then its bispectrum will be equal to zero for all frequency pairs, $C_3^W(\omega_1,\omega_2) = 0$. From Eq. (A.9), it follows that the bispectrum magnitude will be given by,

$$|C_3^Y(\omega_1,\omega_2)| = |\gamma_3^X||H(\omega_1)||H(\omega_2)||H(\omega_1+\omega_2)|$$

and its phase by,

$$\psi_3^Y(\omega_1,\omega_2) = \phi^H(\omega_1) + \phi^H\phi(\omega_2) - \phi^H(\omega_1+\omega_2),$$

where ϕ^H is the phase of $H(\omega)$. Therefore, the bispectrum conserves $H(\omega)$ phase information.

Appendix B. FFT2 based algorithm for computing bicepstrum

Bicepstrum is defined as the inverse 2D z-transform of log bispectrum [27], as follows:

$$b_H(n,m) = Z_2^{-1}[\log[C_3^H(\omega_1,\omega_2)]].$$

Defining $B_h(\omega_1,\omega_2) = \log[C_3^h(\omega_1,\omega_2)]$, and taking partial differentiation we obtain,

$$\frac{\partial B_H(\omega_1,\omega_2)}{\partial\omega_1} = \frac{1}{C_3^H(\omega_1,\omega_2)}\frac{\partial C_3^H(\omega_1,\omega_2)}{\partial\omega_1}$$

or

$$C_3^H(\omega_1,\omega_2)\frac{\partial B_H(\omega_1,\omega_2)}{\partial\omega_1}\omega_1 = \frac{\partial C_3^H(\omega_1,\omega_2)}{\partial\omega_1}\omega_1. \tag{A.10}$$

From Eq. (A.10) it follows that third-order moment sequence, $m_3^H(n,m)$, is related to bicepstrum, $b_H(n,m)$, by the following convolutional formula [27]:

$$-n \cdot m_3^H(n,m) = m_3^H(n,m) * [-m b_h(n,m)]. \tag{A.11}$$

According to Eqs. (A.10) and (A.11) the bicepstrum can be evaluated by Eq. (14), which is presented below again for convenience,

$$n \cdot b_H(n,m) = F_2^{-1}\left\{\frac{F_2[n \cdot m_3^H(n,m)]}{F_2[m_3^H(n,m)]}\right\}.$$

Therefore, the FFT2 based algorithm steps are,

1. Segment data into K records of M samples and subtract the average value of each record.
2. For each of the records, estimate third-order moment sequence, $m_3^H(n,m)$,

$$m_3^H(n,m) = \frac{1}{M}\sum_{k=s_1}^{s_2} x(k)x(k+m)x(k+n),$$

   where

$$s_1 = \max(0, -m, -n)$$
$$s_2 = \min(M-1, M-1-m, N-1-n)$$
$$\text{with } |m| \leqslant L_1, |n| \leqslant L_1,$$

   L_1 determining the region of support for the estimated third-order moment sequence.
3. Average estimates moment sequences of all records and obtain the 2D FFT, for $F_2[n \cdot m_3^H(n,m)]$ and for the estimated third-order moment sequence, $m_3^H(n,m)$.
4. Compute bicepstrum coefficients by Eq. (14).
5. Obtain cepstral parameters by Eq. (10), from bicepstrum coefficients.
6. Initialise $i(0) = o(0) = 1$ and evaluate maximum, $o(k)$, and minimum phase, $i(k)$, IR according to recursive Equations (8a) and (8b).
7. Compute estimated system IR by convolving $o(k)$ and $i(k)$.

References

[1] D.A. Dornfeld, Process monitoring and control for precision manufacturing, Production Engineering 6 (1999) 29–34.
[2] P. Grabec, P. Leskovar, Acoustic emission of a cutting process, Ultrasonics 15 (1977) 17–20.
[3] K. Iwata, T. Moriwaki, Application of acoustic emission measurement to in-process sensing of tool wear, Annals of the CIRP 26 (1977) 19–23.
[4] D.A. Dornfeld, E. Kannatey-Asibu Jr., Acoustic emission during orthogonal metal cutting, International Journal of Mechanical Sciences 22 (1980) 285–296.
[5] D.A. Dornfeld, In process recognition of cutting states, Japan Society of Mechanical Engineers International Journal 37 (1994) 638–650.
[6] A. Iturrospe, V. Atxa, J.M. Abete, Estado del arte de las técnicas de tratamiento de la señal aplicadas a la monitorización de procesos de corte mediante Emisiones Acústicas, XIV Congreso de Máquinas-Herramienta y Tecnologías de Fabricación (INVEMA), Vol. 1, San Sebastián, Spain, October 2002, pp. 259–277.

[7] X. Li, A brief review: acoustic emission method for tool wear monitoring during turning, International Journal of Machine Tools and Manufacture 42 (2002) 157–165.
[8] S.S. Rangwala, D.A. Dornfeld, A study of acoustic emission generated during orthogonal metal cutting—Part 2: spectral analysis, International Journal of Mechanical Sciences 33 (1991) 489–499.
[9] H.K. Tönshoff, M. Jung, S. Männel, W. Rietz, Using acoustic emission signals for monitoring of production processes, Ultrasonics 37 (2000) 681–686.
[10] R. Du, D. Yan, M.A. Elbestawi, Time-frequency distribution of acoustic emission signals for tool wear detection in turning, Proceedings of the Fourth World Meeting on Acoustic Emission, Boston, MA, September 1991.
[11] S.V. Kamarthi, S.R.T. Kumara, P.H. Cohen, Flank wear estimation in turning trough wavelet representation of acoustic emission signals, Journal of Manufacturing Sciences for Engineering 122 (2000) 12–19.
[12] D. Rouby, P. Fleischmann, P. Gobin, An acoustic emission source model based on dislocation movement, Internal friction and ultrasonic attenuation in solids, Internal Friction and Ultrasonic Attenuation in Solids, University of Tokyo Press, Tokyo, Japan, 1977.
[13] V. Belyi, O. Kholodilov, A. Sviridyonok, Acoustic spectrometry as used for evaluation of tribological systems, Wear 69 (1981) 309–319.
[14] J.J. Liu, D.A. Dornfeld, Modeling and analysis of acoustic emission in diamond turning, Journal of Manufacturing Science and Engineering 118 (1996) 199–207.
[15] R.W.B. Stephens, A.A. Pollock, Waveforms and frequency spectra of acoustic emission, Journal of the Acoustical Society of America 50 (1971) 904–910.
[16] D.R. James, S.H. Carpenter, Relationship between acoustic emission and dislocation kinetics in crystalline solids, Journal of Applied Physics 42 (1971) 4685–4697.
[17] H. Hatano, Quantitative measurements of acoustic emission related to its microscopic mechanisms, Journal of the Acoustical Society of America 57 (1975) 639–645.
[18] M.I.L. Pumarega, R. Piotrkowski, J.E. Ruzzante, Discussion of the log-normal distribution of amplitudes in acoustic emission signals, Journal of Acoustic Emission 17 (1999) 61–67.
[19] J.P. Daniel, Application of quantitative acoustics in monitoring precision manufacturing, Ph.D. Dissertation, University of California, Berkeley, 1994.
[20] J. Gary, M. Hamstad, On the far-field structure of waves generated by a pencil break on a thin plate, Journal of Acoustic Emission 12 (1994) 157–170.
[21] L.W. Schmerr Jr., Fundamentals of Ultrasonic Non-destructive Evaluation. A Modeling Approach, Plenum Pub Corp., New York, 1998.
[22] S.K. Sin, C.H. Chen, A comparison of deconvolution techniques for the ultrasonic non-destructive evaluation of materials, IEEE Transactions on Image Processing 1 (1992) 3–10.
[23] A.V. Oppenheim, R.W. Shaffer, Discrete-Time Signal Processing, Prentice-Hall, Englewood Cliffs, NJ, 1989.
[24] C.L. Nikias, A.T. Petropulu, Higher-order Spectra Analysis: A Nonlinear Signal Processing Framework, Prentice-Hall, Englewood Cliffs, NJ, 1993.
[25] J.M. Tribolet, Seismic Applications of Homomorphic Signal Processing, Prentice-Hall, Englewood Cliffs, NJ, 1979.
[26] J.A. Rice, S.M. Wu, Acoustic emission source and transmission path characterization through homomorphic, Journal of Engineering for Industry 116 (1994) 32–41.
[27] A. Yamani, M. Bettayeb, L. Ghouti, Higher-order statistics-based deconvolution of ultrasonic nondestructive testing signals, IEEE Signal Processing Workshop on Higher-Order Statistics (SPW-HOS '97), Banff, Canada, July 21–23, 1997.
[28] M.J. Hinich, Testing for Gaussianity and linearity of stationary time series, Journal of Time Series Analysis 3 (1982) 169–176.
[29] W.B. Lee, C.F. Cheung, S. To, Materials induced vibration in ultra-precision machining, Journal of Materials Processing Technology 89–90 (1999) 318–325.